Global patterns and drivers of C:N:P in marine ecosystems

Tatsuro Tanioka
University of California, Irvine https://orcid.org/0000-0003-2794-7678
Catherine Garcia
University of Hawaii at Manoa
Alyse Larkin
University of California, Irvine
Nathan Garcia
University of California, Irvine
Adam Fagan
University of California, Irvine
Adam Martiny (amartiny@uci.edu)
University of California, Irvine https://orcid.org/0000-0003-2829-4314

Article

Keywords:

Posted Date: February 25th, 2022

DOI: https://doi.org/10.21203/rs.3.rs-1344335/v1

Version of Record: A version of this preprint was published at Communications Earth & Environment on November 7th, 2022. See the published version at https://doi.org/10.1038/s43247-022-00603-6.

Global patterns and drivers of C:N:P in marine ecosystems

Tatsuro Tanioka[1], Catherine A. Garcia[1,3], Alyse A. Larkin[1], Nathan S. Garcia[1], Adam J. Fagan[1], and Adam C. Martiny[1,2,*]

[1] Department of Earth System Science, University of California, Irvine, California 92697, USA
[2] Department of Ecology and Evolutionary Biology, University of California, Irvine, California 92697, USA
[3] Center for Microbial Oceanography: Research and Education (C-MORE), University of Hawaii at Manoa, Honolulu, Hawaii 96822, USA
[*] Corresponding author (amartiny@uci.edu)

The coupling between oceanic carbon-nitrogen-phosphorus (CNP) cycles is a fundamental component of ocean ecosystems. It is now widely recognized that CNP stoichiometry of marine ecosystems is variable through space and time. However, several competing hypotheses have been proposed invoking unique biochemical mechanism and associated environmental drivers to describe the observed patterns. We here quantified the detailed hydrography, plankton genomic diversity, and particulate organic matter to understand the global biogeography of ecosystem CNP stoichiometry across 1370 stations as part of Bio-GO-SHIP. We observed clear latitudinal variability in CNP and show that surface temperature is responsible for much of the stoichiometric variability at high latitudes. Genomic observations allowed us to separate each elemental stress type and revealed that the interaction between nutrient supply rate and N vs. P stress is critical for hemispheric and regional CNP variability. Future climate projections suggest that C:P and N:P ratios will increase at high latitudes, but changes are highly uncertain at low latitudes due to a lack of observations at extreme surface ocean temperature and possible shifts in N vs. P stress. Our observations suggest a systematic regulation of elemental stoichiometry among ocean ecosystems, but future changes are highly uncertain.

Carbon-Nitrogen-Phosphorus (CNP) stoichiometry has been widely used in ocean studies to provide critical linkages between the availability of key nutrients, primary productivity, and carbon sequestration[1,2]. CNP ratios of suspended and exported particulate organic matter (POM) in the surface ocean, reflecting the ecosystem elemental composition, are commonly below the canonical Redfield ratio of 106:16:1 in the cold, nutrient replete high-latitude regions and above the Redfield ratios in the warm, nutrient deplete subtropical gyres[3–5]. Observed CNP ratios also display temporal variability on daily[6], seasonal[7], and inter-annual timescales[8,9]. As changes in CNP ratios can have cascading effects on the carbon cycle[10,11], nitrogen cycle[12,13], and marine food-web dynamics[14], identifying the environmental drivers of CNP has become a pressing challenge.

There are several competing hypotheses for mechanisms controlling marine ecosystem CNP[15–17]. Temperature and nutrients can modulate cellular CNP of phytoplankton through phenotypic and genomic changes on the timescales of days to weeks[18,19]. Furthermore, change in the plankton biodiversity resulting from temperature and nutrient variations can alter bulk ecosystem CNP[20,21] because different taxonomic lineages of plankton have unique optimal CNP[22]**.** The challenge is that temperature and nutrients can explain current field observations equally well due to the

strong apparent latitudinal co-variance between temperature and nutrients, stemming from limited spatial coverage[11,23]. Furthermore, previous global synthesis studies[3,11] relied on dissolved nitrate and phosphorus concentrations to measure nutrient stress, but these nutrients are often below the detection limit in many low latitude ecosystems[24], prohibiting accurate diagnosis of N vs. P limitation[25]. The nutrient limitation type of phytoplankton (e.g., N vs. P limitation) is critical as phytoplankton C:P and N:P cellular ratios can vary by as much as a factor of three between P-limited and N-limited conditions under otherwise the same growth environment[26,27]. As a result of these shortcomings, we still lack a quantitative understanding of what drives marine ecosystem CNP stoichiometry.

Here, we quantify the global variation and identify key environmental drivers for surface ocean CNP based on large-scale systematic measurements of POM. We collected and analyzed new POM samples across all major ocean basins as part of the biological initiative for the Global Ocean Ship-based Hydrographic Investigations Program or Bio-GO-SHIP[28,29] (Fig. 1). The new Bio-GO-SHIP dataset greatly expanded the spatial coverage from the previous global CNP studies[3,30], and now includes samples from regions like the Southern Subtropical Pacific, South Atlantic, and the Indian Ocean. We derived the statistical relationships between CNP with diverse environmental predictors, including nutrient stress of phytoplankton, derived from paired *in situ* metagenomics observations[31]. Finally, we used our data-derived statistical models to project surface ecosystem CNP for the historical period (years, 2010-2014) and end of the 21st

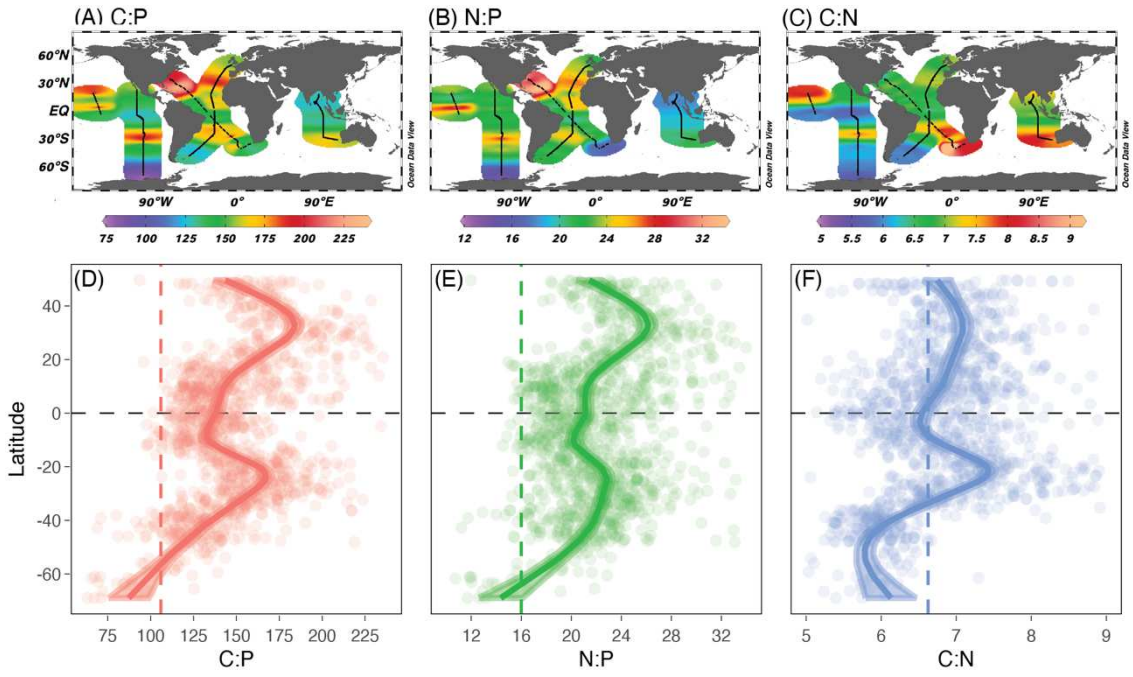

Fig. 1: Global distribution and latitudinal trends of surface ecosystem CNP. (**a-c)** Individual sampling locations are shown with black points in the global map of C:P, N:P, and C:N. Multi-color shadings in (**a**) – (**c**) are based on weighted-average gridding from Ocean Data View. (**d-f)** *In situ* measurements of C:P, N:P, and C:N are plotted against latitude and solid lines represent the GAM smooth trends and ribbons corresponding to the 95% confidence intervals of latitudinal trends predicted by the GAMs. The dotted vertical lines show the canonical CNP Redfield ratio of 106:16:1.

century (years, 2095-2100, shared socioeconomic pathways SSP3-7.0) to identify areas that may undergo the most drastic change in ocean elemental stoichiometry.

Results

We collected 1370 paired POM samples (C, N, and P) in the top 30 m across a broad latitudinal range from 70°S to 55°N (Fig. 1, Supplementary Table 1) and analyzed them using consistent protocols. The global area-weighted mean C:N:P was 148:22:1 (Supplementary Table 2), which agrees with the previous data compilation of surface ecosystem C:N:P of 146:20:1[3]. Ecosystem CNP ratios exhibited a robust latitudinal pattern being highest in the subtropical gyres, intermediate in equatorial regions, and low towards higher latitudes (Fig. 1, Supplementary Table 4). The highest C:P and N:P were observed in the western North Atlantic, where mean values reached 225 and 32, respectively. The lowest values were observed in areas poleward of the Southern subtropical convergence with the lowest observed C:P and N:P ratios of ~60 and ~12, respectively. The latitudinal trends in C:P and N:P were mirrored in both hemispheres, but peak C:P and N:P ratios were commonly higher in the Northern vs. Southern Hemisphere. C:N was close to the canonical Redfield ratio of 6.6 in most regions but noticeably elevated in the southern subtropical gyres in the Atlantic, Indian, and Pacific Ocean with a mean C:N of ~9. In contrast, C:N was slightly lower than the Redfield ratio in the Southern Ocean, with a mean of ~6. Thus, CNP showed a latitudinal gradient but also clear hemisphere deviations.

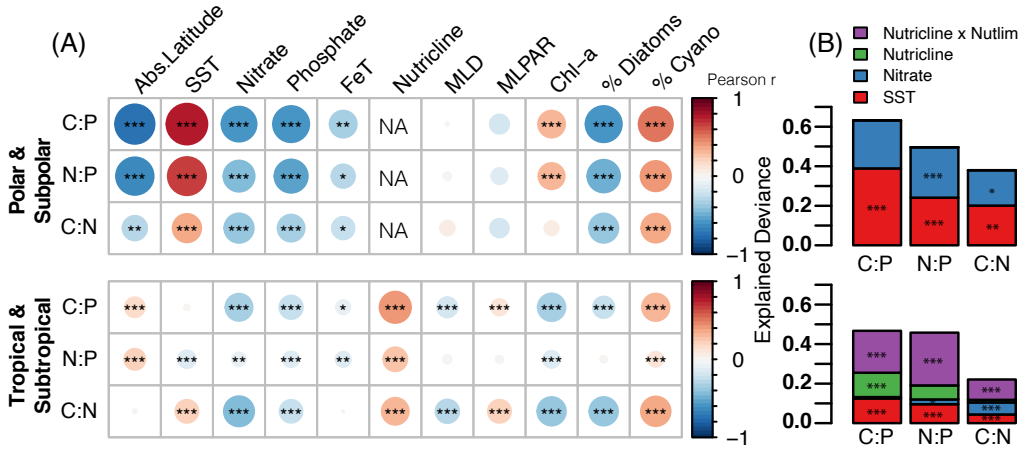

Fig. 2: Drivers of ecosystem CNP. (**a**) Correlation of contextual variables with the CNP ratios. The color gradient and the size of circles are the Pearson *r* correlation coefficient. Asterisks represent the statistical significance (***: $p < 0.001$, **: $p < 0.01$, *: $p < 0.05$, NA: Not Applicable). (**b**) The individual explained deviance and additive contribution of the four main contextual variables to the total explained deviance in generalized additive models (GAMs). In both (**a**) and (**b**), the top half corresponds to the data collected in the (sub)polar regions with |Latitude| ≥ 45° ($n = 139$), and the bottom half corresponds to the data collected in the (sub)tropical regions with |Latitude| < 45° ($n = 1156$).

The dominant environmental predictors of surface ecosystem CNP differed between high and low latitude regions (Fig. 2). In (sub)polar regions, SST was strongly positively correlated with C:P and N:P (Fig. 2a), and SST together with surface nitrate concentration captured 63% and 50% of the total high latitude C:P and N:P variances, respectively (Fig. 2b, Supplementary Table 7). C:P and N:P increased linearly from the coldest polar regions to the warmer subpolar regions, coinciding with a gradual community composition shift from diatom to cyanobacteria dominance (Fig. 2a). Nitrate concentrations corresponded to the general latitudinal trend of C:N across high latitudes, explaining a C:N increase from ~5 in the nitrate-rich polar regions to ~7 in temperate regions (Fig. 3h). Phosphate and nitrate showed strong co-variance (r = 0.92, Pearson), but phosphate was not as good of a predictor for C:N as nitrate. Nutricline depth, where deeper nutricline indicates a lower nutrient supply rate to the upper mixed layer of the ocean[32,33], could not explain variances in CNP as the nutricline depths were uniformly 0 m in these high latitude ecosystems (Extended Data Fig. 1a). Similarly, the element-specific nutrient stress (i.e., N vs. P vs. Fe stress) could not explain CNP variability in the high latitude because regions from which samples were collected were uniformly Fe-limited (Extended Data Fig. 2a). Overall, temperature

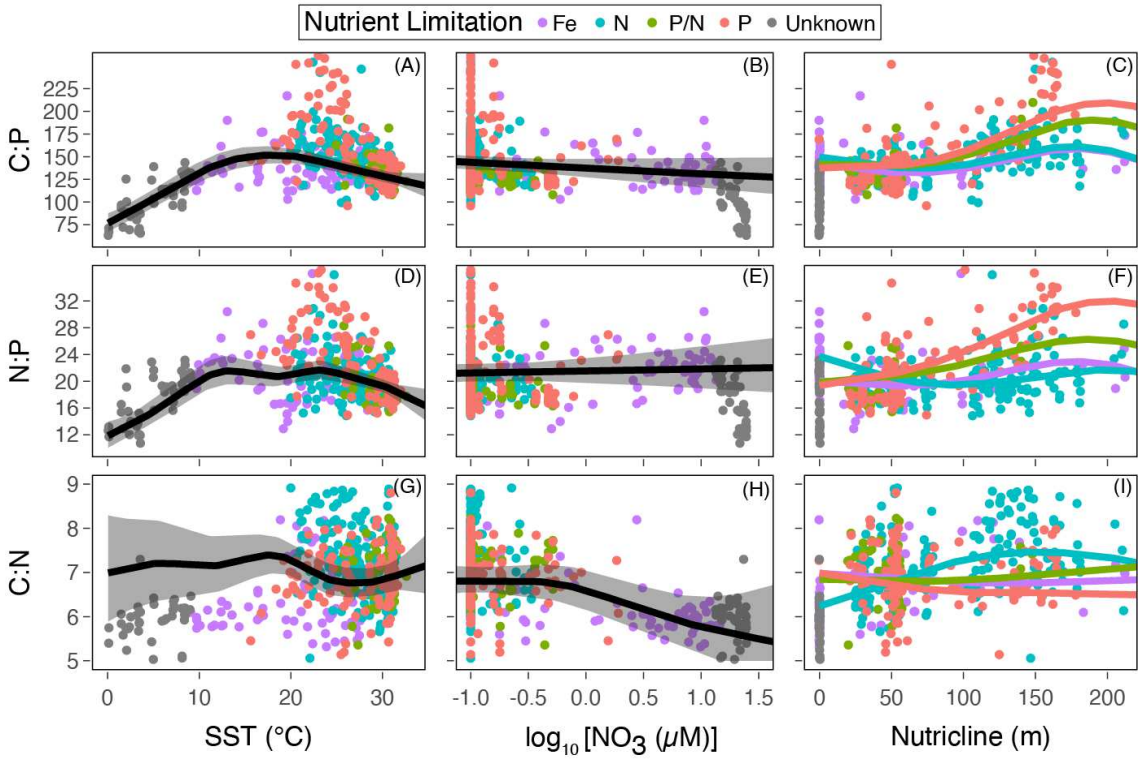

Fig. 3: Observed CNP as a function of environmental variation. Dots are observed values and colors represent the nutrient limitation type inferred from metagenomes (Purple = Fe-limited, Blue = N-limited, Green = P/N co-limited, Red = P-limited, Grey = Unknown). (**a, d, g**) CNP against SST. Black line and shade represent GAM prediction and uncertainty (± 2SE) under the constant nutricline depth and surface nitrate values at the observed mean values of 68 m and 0.3 μM, respectively. (**b, e, h**) CNP against surface nitrate. For GAM prediction, SST and nutricline are kept constant at the observed mean values of 25 °C and 68 m, respectively. (**c, f, i**) CNP against nutricline depth. GAM is fitted separately for each limiting nutrient type under constant SST and surface nitrate at the observed mean values. Uncertainties for GAMs in (**c, f, i**) are provided in Extended Fig. 3-5.

was a primary driver of CNP variability in high latitudes, while macronutrient availability had a lesser, though non-negligible, impact.

In (sub)tropical ecosystems, nutricline depth and the element-specific nutrient stress were the strongest environmental predictors for CNP (Fig. 2b, Supplementary Table 8). GAMs predicted that C:P and N:P increased monotonically with warming until ~20 °C and then plateaued and possibly mildly declined in warm (sub)tropical ecosystems (Fig. 3a, d). Above ~20 °C, we observed that most of the deviance for C:P and N:P were attributed to the nutricline depth plus element-specific nutrient stress. C:P, N:P, and C:N were all significantly positively correlated with nutricline, and regions with deep nutricline corresponded to areas where cyanobacteria dominated (Fig. 2a). C:P and N:P were highest when the nutricline was deeper than 100 m, and phytoplankton were P-stressed or P/N co-stressed (Fig. 3c, f, Extended Data Fig. 3-4). In contrast, C:N was highest when the nutricline was deep, and phytoplankton were N-stressed (Fig. 3i, Extended Data Fig. 5). Nitrate nor phosphate concentrations could not explain much of the CNP variability because observed macronutrient concentrations were at or below detection limits in nearly all the low latitude ecosystems[24]. In summary, the global synthesis of surface ecosystem CNP revealed a transition from a strong temperature dependency at high latitudes to a multi-dimensional nutrient stress control in mid-to-low latitudes.

We next predicted the global distributions of surface CNP stoichiometry by combining the observation-constrained GAMs with projections of present and future oceanic conditions (Fig. 4,

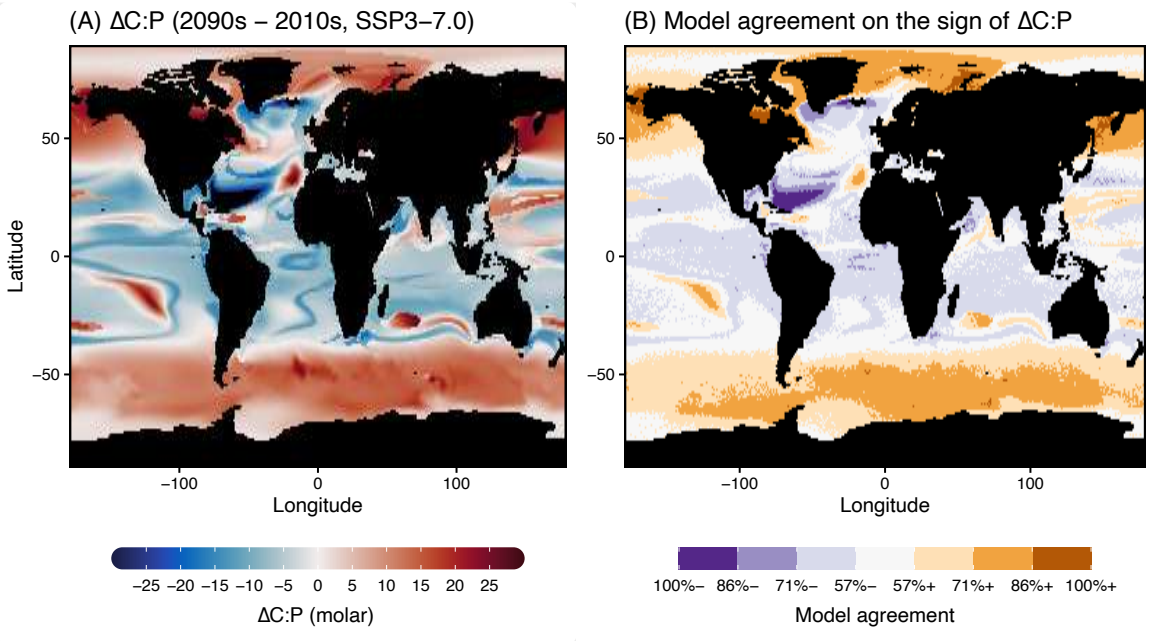

Fig. 4: Projected impact of climate change on the surface ecosystem C:P. (**a**) Difference in surface ecosystem C:P estimated for the 2090s and 2010s based on SST, surface nitrate concentration, nutricline, and nutrient limitation type of small phytoplankton simulated under the SSP3-7.0 and historic CMIP6 scenarios, respectively. (**b**) Model agreement on the sign of change in C:P amongst 2000 randomly generated model projections based on the posterior distribution of the GAM parameters. 100%+ represents the case when all 2000 models predict the positive change in C:P, and 100%- represents the case when all models predict the negative change in C:P. Note that 50%+/50%- corresponds to the minimum agreement between 2000 models.

Extended Data Fig. 6-7). We projected a general increase in C:P at high latitudes but a decrease in the subtropics and tropics (Fig. 4a). This spatial pattern was similar for N:P (Extended Data Fig. 8). Overall, the global area-weighted mean C:N:P changed little from 128:20:1 in the 2010s to 129:19:1 in the 2090s (Supplementary Table 9). Area-weighted mean C:P poleward of 45° increased by ~10 from 94 in the 2010s to 104 in the 2090s. This high latitude increase was predominantly due to a 2-3°C warming (Extended Data Fig. 6c, 9a). In the mid-low latitudes (equatorward of 45°), C:P decreased slightly from 143 in the 2010s to 139 in the 2090s. This decrease in C:P was also driven by warming (Extended Data Fig. 9) as the observation suggested a slight decrease in C:P above ~20 °C (Fig. 3a). However, there are large geographical differences leading to regions with strong declines (e.g., western North Atlantic due to a shoaling nutricline) or increases (e.g., western North Pacific shifting to P-limitation and South Pacific with a deepening nutricline). Moreover, model agreement in the mid-low latitudes rarely exceeded 70% (Fig. 4b). Regions with the lowest model agreement corresponded to areas with the smallest projected change in C:P, such as the boundary between subpolar and subtropics, where the present-day annual mean SST was 15-20 °C. Here, the data-derived slope of SST vs. C:P was relatively flat and the nutricline depths were shallow (Fig. 3a, c); hence neither warming nor change in nutricline had sizable impacts on C:P. Overall, our model projections suggested distinct stoichiometric responses in the high and low latitude ecosystems under the future climate scenario, but regional CNP shifts counteracted each other leading to a small overall global change.

Discussion

Our global analysis revealed an emergent link between temperature, nutricline, element-specific nutrient stress, and CNP stoichiometry. A strong temperature dependency of C:P and N:P in high latitude ecosystems is consistent with the 'Translation Compensation' hypothesis[17,34], where plankton increase allocation to P-rich ribosomes for biosynthesis at low temperature, leading to lower C:P and N:P. The lower temperature also leads to lower C:N of phytoplankton by slowing down the metabolism of phytoplankton and decreasing their ability to consume nitrate, thus increasing residual nitrate concentrations[35]. The transition from a strong temperature dependency at higher latitudes to a strong nutrient dependency at low latitudes may be due to a weakened temperature control on phytoplankton growth under low nutrient supply rate conditions[36,37]. Thus, our data strongly support the 'Translation Compensation' hypothesis and the strong temperature dependency on CNP but only in nutrient-replete environments.

In low latitude ecosystems, we observed a strong regulation from the interaction between the nutricline depth and elemental nutrient stress type. There is strong support in theoretical and culture experiments for this multi-dimensional nutrient control of CNP. Chemostat models predict a more flexible stoichiometry of phytoplankton cells at lower nutrient supply and growth but a fixed CNP at μ_{max}[26,38]. Similarly, culture experiments showed that cellular CNP is very sensitive to N vs. P stress at low growth rates, but this flexibility narrows with higher growth rates[27,39]. Although we could not directly measure nutrient supply, a deeper nutricline reflects a lower overall nutrient supply rate[33]. Thus, the observed interactive regulation of CNP by nutricline depth and N vs. P stress aligns well with these theoretical and culture predictions.

We observed a mild decrease in C:P and N:P in low latitude ecosystems at high temperatures above 20 °C. This may be related to an increase in cellular RNA content to meet a greater

demand of chaperones required for the repair of heat-induced damage[18], or to the disproportionate increase in the respiration over photosynthesis leading to lower carbon fixation at higher temperature[40]. However, we currently lack the observations from regions with the surface temperature above 30˚C to fully constrain the relationship between warming and CNP. In addition to cellular level changes in CNP, low latitude ecosystems also typically favor slow-growing cyanobacteria with higher C:P and N:P ratios over eukaryotes with lower stoichiometric ratios[20,41]. Indeed, we globally observed a significant positive correlation between C:P and N:P with % cyanobacteria (Fig. 2a). However, hemisphere differences in CNP rule out that community shifts alone control the observed CNP.

An inter-hemisphere contrast in ecosystem CNP in low latitude ecosystems may be linked to differences in the N:P:Fe supply ratio and the relative degree of N vs. P stress[6]. More pronounced C:P and N:P peaks were observed in the northern vs. southern hemisphere subtropical gyres. We associate the higher ecosystem C:P and N:P in the northern hemisphere to a more substantial surface phosphate depletion in the North Atlantic and Pacific gyres from the higher Fe supply and N_2 fixation[24]. In contrast, we more commonly observed regions of high C:N in the Southern Hemisphere, including eastern South Atlantic, eastern South Pacific, and the South Indian Oceans. These regions are strongly N-stressed regions with a low Fe supply and low N_2 fixation[12,42,43]. In summary, nutrient supply rate and ratios are likely to be the primary driver of large CNP variability in low latitude marine ecosystems, while temperature and macronutrient availability are responsible for shaping the overall latitudinal gradient.

Our data-driven model projection suggests that future global average C:P and N:P changes may be less drastic than previously estimated[14,34]. However, there are several important caveats to this conclusion. First, despite sampling many ocean regions as part of Bio-GO-SHIP, we still do not have data for several key regions and thus lack analog conditions for low temperature and nutrient stressed as well as regions with surface temperature above 30˚C. Thus, we suggest prioritizing sampling in Arctic Ocean regions with low temperature and depressed nutrients or the extremely warm western Pacific Ocean. Second, a change in the nutrient supply ratio could lead to an abrupt shift in plankton community composition[44], which in turn may abruptly shift ecosystem CNP. Such changes in nutrient supply ratios may be driven by anthropogenic N emission[45], shifting nitrogen fixation[46], and atmospheric nutrient deposition[47]. As these abrupt ecological shifts are expected to precede early warning signals from temperature and nutrients[44], it is critical to expand monitoring of ecosystem CNP through long-term monitoring[7,48], shipboard measurements[29], and remote sensing[49]. These spatial and temporal sampling efforts are critical for narrowing down the degree of uncertainty in model projections of CNP.

References

1. Redfield, A. C., Ketchum, B. H. & Richards, F. A. The influence of organisms on the composition of Seawater. in *The composition of seawater: Comparative and descriptive oceanography. The sea: ideas and observations on progress in the study of the seas* (ed. Hill, M. N.) vol. 2 26–77 (Interscience Publishers, 1963).
2. Deutsch, C. & Weber, T. Nutrient Ratios as a Tracer and Driver of Ocean Biogeochemistry. *Ann. Rev. Mar. Sci.* **4**, 113–141 (2012).
3. Martiny, A. C. *et al.* Strong latitudinal patterns in the elemental ratios of marine plankton

and organic matter. *Nat. Geosci.* **6**, 279–283 (2013).
4. Quay, P. Impact of the Elemental Composition of Exported Organic Matter on the Observed Dissolved Nutrient and Trace Element Distributions in the Upper Layer of the Ocean. *Global Biogeochem. Cycles* **35**, 1–16 (2021).
5. Teng, Y.-C., Primeau, F. W., Moore, J. K., Lomas, M. W. & Martiny, A. C. Global-scale variations of the ratios of carbon to phosphorus in exported marine organic matter. *Nat. Geosci.* **7**, 895–898 (2014).
6. Garcia, C. A. *et al.* Nutrient supply controls particulate elemental concentrations and ratios in the low latitude eastern Indian Ocean. *Nat. Commun.* **9**, 4868 (2018).
7. Singh, A. *et al.* C : N : P stoichiometry at the Bermuda Atlantic Time-series Study station in the North Atlantic Ocean. *Biogeosciences* **12**, 6389–6403 (2015).
8. Karl, D. M. *et al.* Ecological nitrogen-to-phosphorus stoichiometry at station ALOHA. *Deep Sea Res. Part II Top. Stud. Oceanogr.* **48**, 1529–1566 (2001).
9. Fagan, A. J., Moreno, A. R. & Martiny, A. C. Role of ENSO Conditions on Particulate Organic Matter Concentrations and Elemental Ratios in the Southern California Bight. *Front. Mar. Sci.* **6**, 386 (2019).
10. Matsumoto, K., Tanioka, T. & Rickaby, R. Linkages Between Dynamic Phytoplankton C:N:P and the Ocean Carbon Cycle Under Climate Change. *Oceanography* **33**, 44–52 (2020).
11. Galbraith, E. D. & Martiny, A. C. A simple nutrient-dependence mechanism for predicting the stoichiometry of marine ecosystems. *Proc. Natl. Acad. Sci.* **112**, 8199–8204 (2015).
12. Wang, W.-L., Moore, J. K., Martiny, A. C. & Primeau, F. W. Convergent estimates of marine nitrogen fixation. *Nature* **566**, 205–211 (2019).
13. Mills, M. M. & Arrigo, K. R. Magnitude of oceanic nitrogen fixation influenced by the nutrient uptake ratio of phytoplankton. *Nat. Geosci.* **3**, 412–416 (2010).
14. Kwiatkowski, L., Aumont, O., Bopp, L. & Ciais, P. The Impact of Variable Phytoplankton Stoichiometry on Projections of Primary Production, Food Quality, and Carbon Uptake in the Global Ocean. *Global Biogeochem. Cycles* **32**, 516–528 (2018).
15. Sterner, R. W. & Elser, J. J. *Ecological stoichiometry: the biology of elements from molecules to the biosphere*. (Princeton University Press, 2002).
16. Allen, A. P. & Gillooly, J. F. Towards an integration of ecological stoichiometry and the metabolic theory of ecology to better understand nutrient cycling. *Ecol. Lett.* **12**, 369–384 (2009).
17. Moreno, A. R. & Martiny, A. C. Ecological Stoichiometry of Ocean Plankton. *Ann. Rev. Mar. Sci.* **10**, 43–69 (2018).
18. Schaum, C.-E., Buckling, A., Smirnoff, N., Studholme, D. J. & Yvon-Durocher, G. Environmental fluctuations accelerate molecular evolution of thermal tolerance in a marine diatom. *Nat. Commun.* **9**, 1719 (2018).
19. Geider, R. & La Roche, J. Redfield revisited: variability of C:N:P in marine microalgae and its biochemical basis. *Eur. J. Phycol.* **37**, 1–17 (2002).
20. Sharoni, S. & Halevy, I. Nutrient ratios in marine particulate organic matter are predicted by the population structure of well-adapted phytoplankton. *Sci. Adv.* **6**, eaaw9371 (2020).
21. Bonachela, J. A., Klausmeier, C. A., Edwards, K. F., Litchman, E. & Levin, S. A. The role of phytoplankton diversity in the emergent oceanic stoichiometry. *J. Plankton Res.* **38**, 1021–1035 (2016).
22. Quigg, A. *et al.* The evolutionary inheritance of elemental stoichiometry in marine

phytoplankton. *Nature* **425**, 291–4 (2003).
23. Yvon-Durocher, G., Dossena, M., Trimmer, M., Woodward, G. & Allen, A. P. Temperature and the biogeography of algal stoichiometry. *Glob. Ecol. Biogeogr.* **24**, 562–570 (2015).
24. Martiny, A. C. *et al.* Biogeochemical controls of surface ocean phosphate. *Sci. Adv.* **5**, eaax0341 (2019).
25. Moore, C. M. *et al.* Processes and patterns of oceanic nutrient limitation. *Nat. Geosci.* **6**, 701–710 (2013).
26. Klausmeier, C. A., Litchman, E. & Levin, S. A. Phytoplankton growth and stoichiometry under multiple nutrient limitation. *Limnol. Oceanogr.* **49**, 1463–1470 (2004).
27. Garcia, N. S., Bonachela, J. A. & Martiny, A. C. Interactions between growth-dependent changes in cell size, nutrient supply and cellular elemental stoichiometry of marine Synechococcus. *ISME J.* **10**, 1–10 (2016).
28. Larkin, A. A. *et al.* High spatial resolution global ocean metagenomes from Bio-GO-SHIP repeat hydrography transects. *Sci. Data* **8**, 107 (2021).
29. Clayton, S. *et al.* Bio-GO-SHIP: The Time Is Right to Establish Global Repeat Sections of Ocean Biology. *Front. Mar. Sci.* **8**, (2022).
30. Martiny, A. C., Vrugt, J. A., Primeau, F. W. & Lomas, M. W. Regional variation in the particulate organic carbon to nitrogen ratio in the surface ocean. *Global Biogeochem. Cycles* **27**, 723–731 (2013).
31. Ustick, L. J. *et al.* Metagenomic analysis reveals global-scale patterns of ocean nutrient limitation. *Science (80-.).* **372**, 287–291 (2021).
32. Richardson, K. & Bendtsen, J. Vertical distribution of phytoplankton and primary production in relation to nutricline depth in the open ocean. *Mar. Ecol. Prog. Ser.* **620**, 33–46 (2019).
33. Cermeno, P. *et al.* The role of nutricline depth in regulating the ocean carbon cycle. *Proc. Natl. Acad. Sci.* **105**, 20344–20349 (2008).
34. Toseland, A. *et al.* The impact of temperature on marine phytoplankton resource allocation and metabolism. *Nat. Clim. Chang.* **3**, 979–984 (2013).
35. Sauterey, B. & Ward, B. A. Environmental control of marine phytoplankton stoichiometry in the North Atlantic Ocean. *Proc. Natl. Acad. Sci.* **119**, e2114602118 (2022).
36. Marañón, E., Lorenzo, M. P., Cermeño, P. & Mouriño-Carballido, B. Nutrient limitation suppresses the temperature dependence of phytoplankton metabolic rates. *ISME J.* **12**, 1836–1845 (2018).
37. Thomas, M. K. *et al.* Temperature–nutrient interactions exacerbate sensitivity to warming in phytoplankton. *Glob. Chang. Biol.* **23**, 3269–3280 (2017).
38. Droop, M. R. The nutrient status of algal cells in continuous culture. *J. Mar. Biol. Assoc. United Kingdom* **54**, 825–855 (1974).
39. Hillebrand, H. *et al.* Goldman revisited: Faster growing phytoplankton has lower N:P and lower stoichiometric flexibility. *Limnol. Oceanogr.* **58**, 2076–2088 (2013).
40. Barton, S. *et al.* Evolutionary temperature compensation of carbon fixation in marine phytoplankton. *Ecol. Lett.* **23**, 722–733 (2020).
41. Weber, T. S. & Deutsch, C. Oceanic nitrogen reservoir regulated by plankton diversity and ocean circulation. *Nature* **489**, 419–422 (2012).
42. Gruber, N. & Sarmiento, J. L. Global patterns of marine nitrogen fixation and denitrification. *Global Biogeochem. Cycles* **11**, 235–266 (1997).

43. Moore, J. K., Doney, S. C. & Lindsay, K. Upper ocean ecosystem dynamics and iron cycling in a global three-dimensional model. *Global Biogeochem. Cycles* **18**, (2004).
44. Cael, B. B., Dutkiewicz, S. & Henson, S. A. Abrupt shifts in 21st-century plankton communities. *Sci. Adv.* **7**, 8593–8622 (2021).
45. Penuelas, J., Janssens, I. A., Ciais, P., Obersteiner, M. & Sardans, J. Anthropogenic global shifts in biospheric N and P concentrations and ratios and their impacts on biodiversity, ecosystem productivity, food security, and human health. *Glob. Chang. Biol.* **26**, 1962–1985 (2020).
46. Jiang, H.-B. *et al.* Ocean warming alleviates iron limitation of marine nitrogen fixation. *Nat. Clim. Chang.* **8**, 709–712 (2018).
47. Krishnamurthy, A., Moore, J. K., Mahowald, N., Luo, C. & Zender, C. S. Impacts of atmospheric nutrient inputs on marine biogeochemistry. *J. Geophys. Res.* **115**, G01006 (2010).
48. Talarmin, A. *et al.* Seasonal and long-term changes in elemental concentrations and ratios of marine particulate organic matter. *Global Biogeochem. Cycles* **30**, 1699–1711 (2016).
49. Tanioka, T., Fichot, C. G. & Matsumoto, K. Toward Determining the Spatio-Temporal Variability of Upper-Ocean Ecosystem Stoichiometry From Satellite Remote Sensing. *Front. Mar. Sci.* **7**, 604893 (2020).

Acknowledgments
We thank the many contributing GO-SHIP researchers for the oceanographic data; J.K. Moore and N.A. Wiseman for sharing CESM simulation results; G. Hagstrom and F. Primeau for providing technical advice; and K. Matsumoto and E. Galbraith for valuable comments and suggestions. We gratefully acknowledge financial support by the Simons Foundation (Postdoctoral Fellowship in Marine Microbial Ecology Award 724483 to T.T), NOAA (101813-Z7554214 to A.C.M), NASA (FINESST to C.A.G and 80NSSC21K1654 to A.C.M), and the National Science Foundation (OCE-1046297, 1559002, 1848576, and 1948842 to A.C.M). The PML AMT is funded by the UK Natural Environment Research Council through its National Capability Long-term Single Centre Science Program, Climate Linked Atlantic Sector Science (grant number NE/R015953/1). This study contributes to the international IMBeR project and is contribution number 376 of the AMT programme.

Author contributions
C.A.G, A.A.L, N.S.G, and A.J.F coordinated sample collection and/or processed samples. C.A.G and T.T compiled metadata. A.C.M designed and supervised the study, secured funding, and coordinated the Bio-GO-SHIP program. T.T conducted data analysis and wrote the manuscript with substantial input from all co-authors.

Competing interests
The authors declare no competing interests

Additional information
Supplementary information is available for this paper.
Correspondence and requests for materials should be addressed to A.C.M.

Data availability

POM, hydrography, and metagenomes from Bio-GO-SHIP cruises used in this study are publicly available[28]. Nutrient stress data of phytoplankton can be accessed from the original publication cited in the main text[31]. GLODAP version2.2016b data is publicly available (https://doi.org/10.5194/essd-8-297-2016). The model output from CEMS2 Large Ensemble Simulation is available here (https://doi.org/10.26024/kgmp-c556).

Code availability

All data (data manipulation, analyses, figures, and tables) can be downloaded from the GitHub repository https://github.com/tanio003/CNPGlobal_paper_repo. When using the data or code from this project, please cite https://doi.org/10.5281/zenodo.6015417.

Methods

POM Sample Collection

In this study, we use paired observations of particulate organic phosphorus (POP), nitrogen (PON), and carbon (POC) samples from 1370 stations collected between 2011 and 2020 as a part of a novel biological initiative for the Global Ocean Ship Based Hydrographic Investigations Program (Bio-GO-SHIP)[28,29]. Samples used in this study are from cruises I09N, C13.5, P18, AMT-28, NH1418, BVAL46, and AE1319 (Supplementary Table 1). Samples were collected across all major oceanic provinces from 70°S to 55°N using the consistent sampling method described previously[6,28,50,51]. Briefly, 8 L seawater for the POM samples was collected from the onboard flow-through underway system at the sea surface (< 30 m) and was divided into POC/PON and POP triplicates after removing large plankton and particles using 30 µm nylon mesh. Each replicate was then filtered on precombusted Whatman GF/F filters with a nominal pore size of 0.7 µm. POP filters were rinsed with 5 mL of 0.17 M Na_2SO_4 prior to analysis to remove traces of dissolved organic phosphorus. All filtered POM samples were sealed in precombusted aluminum packets and were immediately frozen at -20 °C until analysis. The detection limit for POP measurement was ~ 0.3 µg.

POC and PON samples were measured using Control Equipment 240-XA/440-XA elemental analyzer standardized to acetanilide or a CN Flash 1112 EA elemental analyzer against an atropine ($C_{17}H_{23}NO_3$) standard curve. The POC analysis included an acidification step in concentrated HCl fumes to remove particulate inorganic carbonates. POC and PON measurements had a mean detection limit of ~2.4 µg and ~3.0 µg, respectively. POP was analyzed using the ash-hydrolysis colorimetric method described previously[52] using a spectrophotometer at 885 nm.

Following the criteria used in Lee et al. (2021)[51], we discarded any anomalous samples with POC:POP > 500, PON:POP < 1, and PON:POP > 100 after the stoichiometric ratios were calculated. These selection processes led to 1295 final C-N-P paired POM measurements. To evaluate the influence of spatial autocorrelation, we binned the samples into 1° by 1° grid cells and computed globally area-weighted values with this dataset. Our analysis showed that the global area-weighted means of binned and unbinned data are indistinguishable and concluded that such spatial autocorrelation was not a problem in our data analysis (Supplementary Tables 2 and 3). Based on our previous studies[3,30], a large proportion of POM pools collected are assumed to be made up of living planktonic materials consisting of *Prochlorococcus*, *Synechococcus,*

eukaryotic phytoplankton, and bacteria with a minor contribution from microzooplankton and heterotrophic nanoflagellates.

Hydrography Measurements

Hydrographic measurements (salinity, temperature, and pressure) were taken at each station with a vertical profiling system (CTD-rosette). Ambient surface nutrient (nitrate, phosphate, silicate) concentrations were determined onboard using an auto-analyzer following the GO-SHIP nutrient protocol[53]. Detection limits for phosphate and nitrate concentrations were 0.01 and 0.1 μM, respectively. For the C13/A13.5 section which *in situ* nutrient measurements were not measured due to logistical issues, we substituted for missing values with mapped annual mean average values from the GLODAP version2.2016b from the nearest longitude and latitude at 1° resolution[54,55]. We set consistent detection limits for nitrate and phosphate at 0.1 and 0.01 μM, respectively, for all the hydrographic measurements and corrected any measured concentrations below these values are assumed to be equal to the threshold concentrations for use in statistical analysis.

Contextual Environmental Variables

We complemented *in situ* measurements with (i) mixed-layer averaged photosynthetically available radiation (MLPAR) following Brun et al. (2015)[56], which was estimated using PAR, Chl-a, and monthly climatology of mixed layer depth (MLD)[57], (ii) annual mean nutricline depth, a depth at which nitrate equals 1 μM retrieved from GLODAP version2.2016b, (iii) the average phytoplankton community composition (diatoms, coccolithophores, chlorophyte, and cyanobacteria) between 1998-2017, which we obtained from NASA Ocean Biogeochemical Model (NOBM)[58,59], and (iv) the annual mean total dissolved iron (FeT), which we derived from Community Earth System Model v1.2.1. Satellite-based PAR and Chl-a are 8-day averaged values retrieved by NASA MODIS-Aqua at the nearest location (4 km resolution) (http://oceancolor.gsfc.nasa.gov (last access: July 29, 2021)). The model phytoplankton community composition from NASA NOBM data[58,59] only exists for 1998-2017. For data from 2018 onwards, we used the model output from 2004, which is the year with the minimum sum of deviations from the monthly mean, following the previous study[20].

Metagenomics-Informed Nutrient Limitation

We used the previously published global genome content of *Prochlorococcus* and its inferred element-specific nutrient stress[31]. Specifically, we selected data from 466 stations, where metagenomes samples were collected concomitantly with POM (Extended Data Fig. 2a). We collected metagenomes in the regions encompassing 51.5°S and 48.7°N, where the abundance of *Prochlorococcus* was sufficient. Briefly, sequences from the surface metagenomes were recruited to known strains of *Prochlorococcus,* and the frequency of established nutrient acquisition genes determined *a priori* were used as a proxy for nutrient stress type (i.e., limiting nutrient element) and severity. An ordination of nutrient genes based on the angles from the principal component analysis can broadly categorize six types of limitation and co-limitation: (1) Fe limitation, (2) Fe/P co-limitation, (3) P limitation, (4), P/N co-limitation, (5) N limitation, and (6) N/Fe co-limitation. As the number of samples for Fe/P co-limitation and N/Fe co-limitation samples was noticeably smaller than other stress types, we merged Fe/P and N/Fe with P and N limitation samples, respectively. In total, our dataset consists of 121 P-limitation samples, 195 N-

limitation samples, 65 P/N co-limitation samples, and 85 Fe-limitation samples that are geographically paired with POM samples.

Data Analysis and Modeling

All the statistical analyses were conducted using R ver. 4.1.0[60]. To determine the relative importance of different contextual variables required to explain CNP, we first conducted multiple pairwise correlation analyses using the Pearson correlation test, which allowed us to determine a first-order linear relationship between a covariate and CNP. We used natural log-transformed values of elemental stoichiometric ratios and nutrient concentrations in computing Pearson *r*. For fair comparison across variables, we removed from the dataset any rows containing the missing value(s) and standardized all the variables so that the mean equaled zero and the standard deviation equaled one. We correlated CNP with various environmental drivers including *in situ* measurements of SST, surface phosphate, and nitrate concentrations; mixed-layer depth (MLD), mixed-layer averaged PAR, nutricline depth, modeled surface plankton community composition, and total dissolved iron (FeT) from the model simulations (Supplementary Tables 5 and 6). We performed separate analyses for the (1) polar/subpolar (n = 139) and (2) tropical/subtropical regions (n = 1156) which were delineated based on the absolute latitude of 45°.

We subsequently conducted analyses with generalized additive models (GAMs) to identify the relative strength of four main contextual variables in explaining CNP: these were (1) SST, (2) surface nitrate concentration, (3) nutricline depth, and (4) the limiting nutrient type of *Prochlorococcus* determined from the metagenome analysis. We chose these contextual variables based upon the correlation analysis and on the previous understanding of ecological stoichiometry. For the GAM analysis, we used the R package *mgcv*[61]. For GAM analyses in (sub)tropical regions, we used the subset of POM data where both POM and metagenomes were collected (n = 456). We conducted preliminary hierarchical GAM[62] analyses combined with k-fold cross-validation (100 random partitions holding out 20% of observations) and found that the model with the interactive effect of nutricline and element-specific nutrient limitation type outperformed the model with either independent or null effects of nutrient limitation type. Specifically, the model "GS," where all groups based on nutrient limitation types have similar functional responses, but intergroup variation in responses is allowed, outperformed other model types of functional variation for hierarchical GAM[62] (Supplementary Information). Thus, we decided to use the model GS to describe the interaction between nutricline and element-specific nutrient limitation throughout the paper. The additive contribution of each contextual variable (SST, nitrate, nutricline, and the interaction between nutricline and nutrient limitation type) to the total deviance explained was calculated by sequentially removing different parameters and normalizing with a null model. Note that in the (sub)polar regions ($|\text{Latitude}| \geq 45°$), nutricline depth was uniformly 0 m (i.e., surface nitrate concentration exceeded 1 μM) (Extended Data Fig. 1a), and both the observed and modeled phytoplankton nutrient limitation type were uniformly Fe-limited (Extended Data Fig. 2a). Thus, only SST and surface nitrate concentrations explained CNP deviance in (sub)polar regions.

Future Projections of Ecosystem CNP

We first derived the global GAM formulation of CNP covering the entire parameter space of SST, surface nitrate, nutricline, and nutrient limitation. We supplemented POM-metagenome

paired samples with 40 POM-only samples collected in high latitudes poleward of 51.5°S and 48.7°N. In doing so, we assumed that these 40 samples were all collected from Fe-limited regions based on comparison with CESM model output (Extended Data Fig. 2a) and prior biogeochemical knowledge[25].

To evaluate the effects of future climatic change on surface community C:P and N:P, we used as input to our GAM derived above with the values of SST, surface nitrate concentration, nutricline depth, and nutrient limitation output from CESM2 Large Ensemble Simulation (CESM2-LENS), which consists of 100 ensemble model simulations which take into the account of the ocean and atmospheric interannual variabilities. The ensemble simulation includes four independent AMOC states and 20 microstates for each AMOC scenarios[63]. At the time of writing this paper, 90 out of 100 model outputs were publicly available, and we extracted environmental variables for each grid cell for each of the 90 model runs and computed ensemble means for the historic period (averaged values for years 2010-2014) and the end of the 21st century (averaged values for years 2095-2099), the latter considering Shared Socioeconomic Pathway SSP3-7.0 scenario. SSP3-7.0 scenario is the second most pessimistic, high-greenhouse-gas emission IPCC trajectory[64], where CO_2 doubles compared to preindustrial by 2100 and radiative forcing level reaches 7.0 W/m^2. To obtain ensemble mean SST and surface nitrate concentrations for each grid point, we first computed mean values in the top 30 m for each grid point of every model realization and computed ensemble mean. In each model realization, nutricline was determined first by interpolating the vertical depth profile of nitrate to 1 m in the top 500 m of the water column, and then the shallowest depth at which nitrate concentration exceeds 1 μM was determined. After the initial inspection, we found that the nutricline depth obtained from CESM2-LENS systematically underestimated GLODAP (Extended Data Fig. 1). Thus, we multiplied nutricline depth by the scaling factor of 1.54 for every grid point for historical and future projections. The coefficient of determination between GLODAP and CESM2 historic nutricline depth was 0.8 (Extended Data Fig. 1d).

The limiting nutrient for each grid point is defined as the element with the lowest ratio between the ambient nutrient concentration and the Michaelis-Menten half-saturation constant of the respective element for small phytoplankton functional type. We defined P/N co-limitation when the ratios between the ambient nutrient concentration and the Michaelis-Menten half-saturation constant for P and N are within 5% of each other and were not Fe limited. As the nutrient limitation information is a discrete, categorical variable, we computed the ensemble mode across 90 model runs as the representative nutrient limitation for each grid point. Nutrient limitation map from CESM2-LENS for the historic period generally agreed well with the metagenome-based observation[31] (Extended Data Fig. 2a).

To ensure the reliability of our projections, we generated 1000 historic and future C:P and N:P models from the posterior distribution and randomly selected 2000 models with replacement to account for the uncertainties in the parameters of the GAMs. Here, we report averaged predictions from these 2000 models (Extended Data Fig. 7), and we define model confidence by calculating how many of the 2000 pairs of model projections predict the same sign of change in ΔC:P and ΔN:P from the 2010s to 2090s. For example, if all 2000 randomly selected pairs predict an increase (decrease) in C:P, the model confidence is 100%+ (100%-). The null case (i.e., 50% model confidence) is when half of the model pairs predicted an increase, and the other

half predicted a decrease. Note that the model uncertainty only considers the uncertainties in the parameters of GAMs and not the variance associated with the ensembled environmental variables from the CESM2-LENS output.

Methods References

50. Garcia, C. A. *et al.* Linking regional shifts in microbial genome adaptation with surface ocean biogeochemistry. *Philos. Trans. R. Soc. B Biol. Sci.* **375**, 20190254 (2020).
51. Lee, J. A., Garcia, C. A., Larkin, A. A., Carter, B. R. & Martiny, A. C. Linking a Latitudinal Gradient in Ocean Hydrography and Elemental Stoichiometry in the Eastern Pacific Ocean. *Global Biogeochem. Cycles* **35**, (2021).
52. Lomas, M. W. *et al.* Sargasso Sea phosphorus biogeochemistry: An important role for dissolved organic phosphorus (DOP). *Biogeosciences* **7**, 695–710 (2010).
53. Becker, S. *et al.* GO-SHIP Repeat Hydrography Nutrient Manual: The Precise and Accurate Determination of Dissolved Inorganic Nutrients in Seawater, Using Continuous Flow Analysis Methods. *Front. Mar. Sci.* **7**, 908 (2020).
54. Lauvset, S. K. *et al.* A new global interior ocean mapped climatology: the 1° × 1° GLODAP version 2. *Earth Syst. Sci. Data* **8**, 325–340 (2016).
55. Key, R. M. *et al. Global ocean data analysis project, version 2 (GLODAPv2)*. *Ornl/Cdiac-162, Ndp-093* (2015) doi:10.3334/CDIAC/OTG.NDP093_GLODAPv2.
56. Brun, P. *et al.* Ecological niches of open ocean phytoplankton taxa. *Limnol. Oceanogr.* **60**, 1020–1038 (2015).
57. Holte, J., Talley, L. D., Gilson, J. & Roemmich, D. An Argo mixed layer climatology and database. *Geophys. Res. Lett.* **44**, 5618–5626 (2017).
58. Gregg, W. W. & Casey, N. W. Sampling biases in MODIS and SeaWiFS ocean chlorophyll data. *Remote Sens. Environ.* **111**, 25–35 (2007).
59. Gregg, W. W., Ginoux, P., Schopf, P. S. & Casey, N. W. Phytoplankton and iron: validation of a global three-dimensional ocean biogeochemical model. *Deep Sea Res. Part II Top. Stud. Oceanogr.* **50**, 3143–3169 (2003).
60. R Core Team. R: A Language and Environment for Statistical Computing. (2021).
61. Wood, S. N. Fast stable restricted maximum likelihood and marginal likelihood estimation of semiparametric generalized linear models. *J. R. Stat. Soc. Ser. B Stat. Methodol.* **73**, 3–36 (2011).
62. Pedersen, E. J., Miller, D. L., Simpson, G. L. & Ross, N. Hierarchical generalized additive models in ecology: An introduction with mgcv. *PeerJ* **2019**, (2019).
63. Rodgers, K. *et al.* Ubiquity of human-induced changes in climate variability. *Earth Syst. Dyn. Discuss.* 1–22 (2021) doi:10.5194/ESD-2021-50.
64. O'Neill, B. C. *et al.* A new scenario framework for climate change research: the concept of shared socioeconomic pathways. *Clim. Change* **122**, 387–400 (2014).

Extended Data Figures

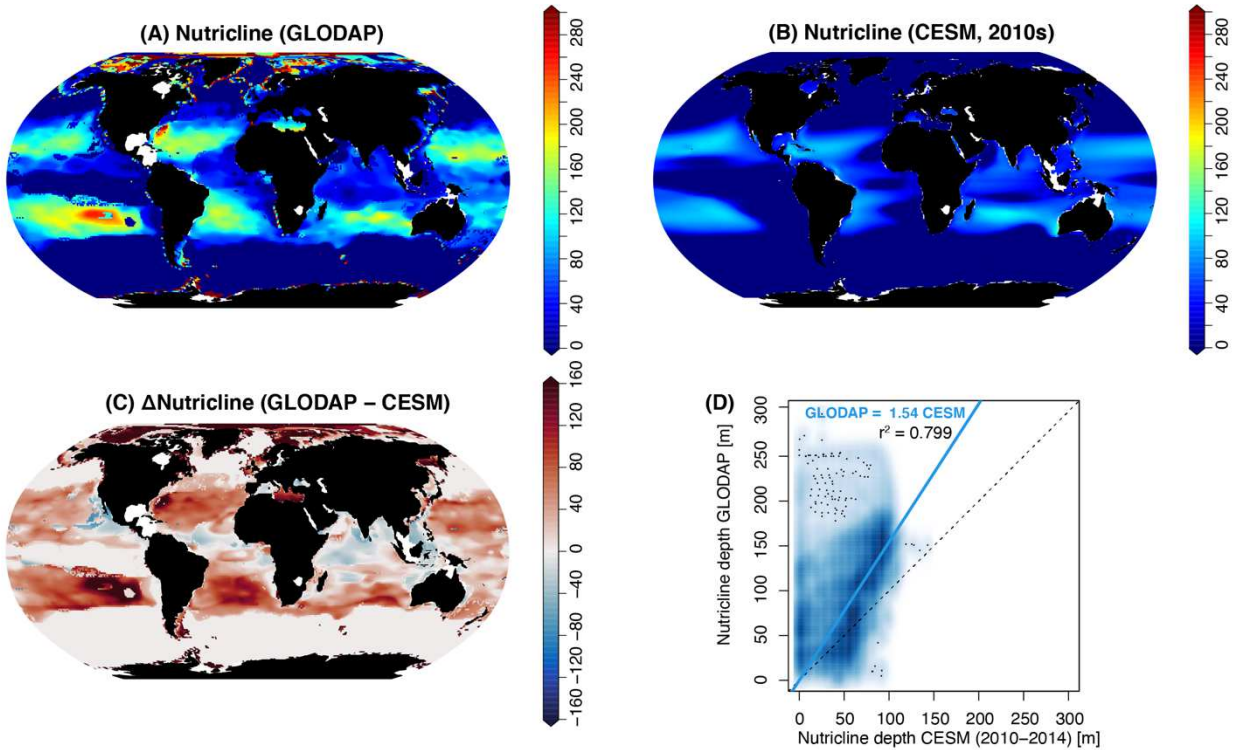

Extended Data Fig. 1: Global map of annual mean nutricline depth. Nutricline depth is defined as a depth at which NO_3 concentration first equals 1 µM. Nutricline is defined as 0 m if NO_3 consistently exceeds the threshold value of 1 µM throughout the water column. (**a**) Mean nutricline depth was determined from the annual mean gridded NO_3 field from GLODAP version2.2016b. (**b**) Ensemble mean nutricline depth across 90 models from CESM2 Large Ensemble Simulation (CESM-LENS) for the historic periods 2010-2014. (**c**) Difference between nutricline depth from panels **(a)** and **(b)**. (**d**) Comparison between GLODAP-based and CESM-based nutricline depth. Note that GLODAP-based nutricline depth is systematically higher than CESM-based nutricline depth with the constant of proportionality of 1.54 (blue line, $r^2 = 0.799$).

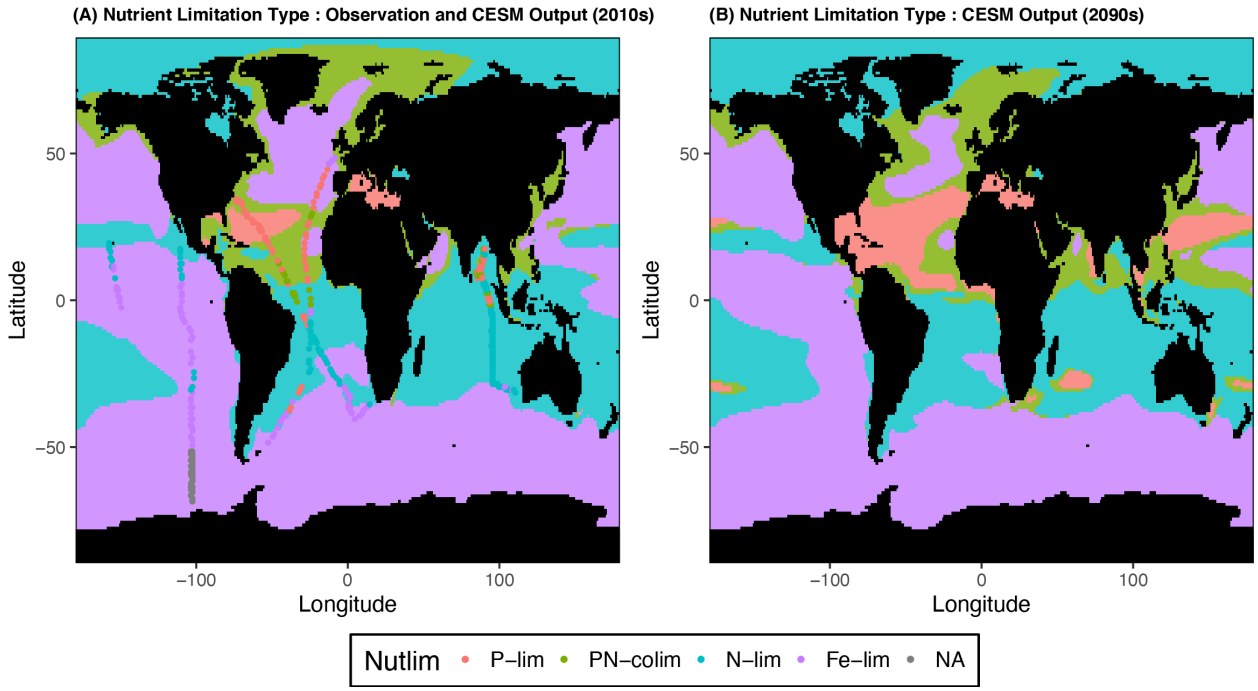

Extended Data Fig. 2: Global map of observed and modeled nutrient limitation type for small phytoplankton type. Different colors indicate different nutrient limitation types, and the dots are metagenome-derived nutrient limitation types[31] for corresponding stations in which POM samples were collected (Purple = Fe-limited, Blue = N-limited, Green = P/N co-limited, Red = P-limited, Grey = Not Applicable). Shadings are based on nutrient limitation of small phytoplankton types from CESM2-LENS for (**a**) the 2010s and (**b**) the 2090s under SSP3-7.0.

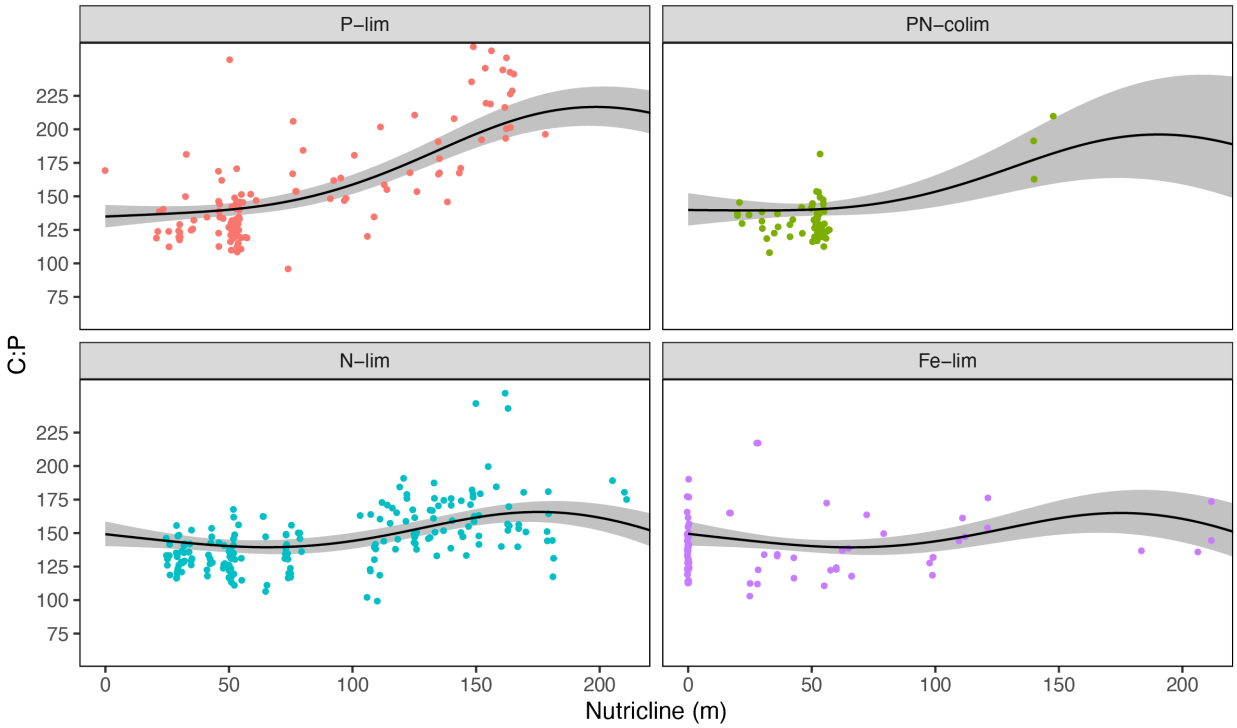

Extended Data Fig. 3: Observed C:P as a function of nutricline depth and nutrient limitation types. The figure is identical to main Fig. 3c but highlights the uncertainty (± 2SE) associated with GAM predictions under the constant SST and surface nitrate values.

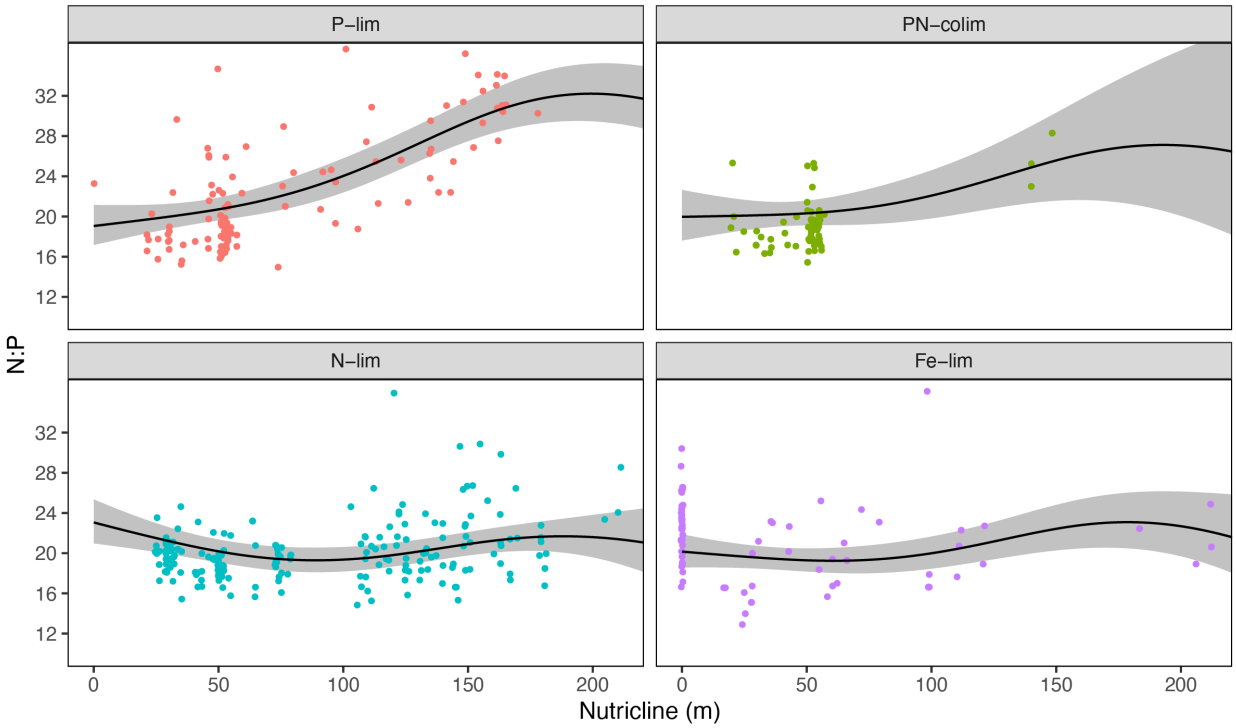

Extended Data Fig. 4: Observed N:P as a function of nutricline depth and nutrient limitation types. The figure is identical to main Fig. 3f but highlights the uncertainty (± 2SE) associated with GAM predictions under the constant SST and surface nitrate values.

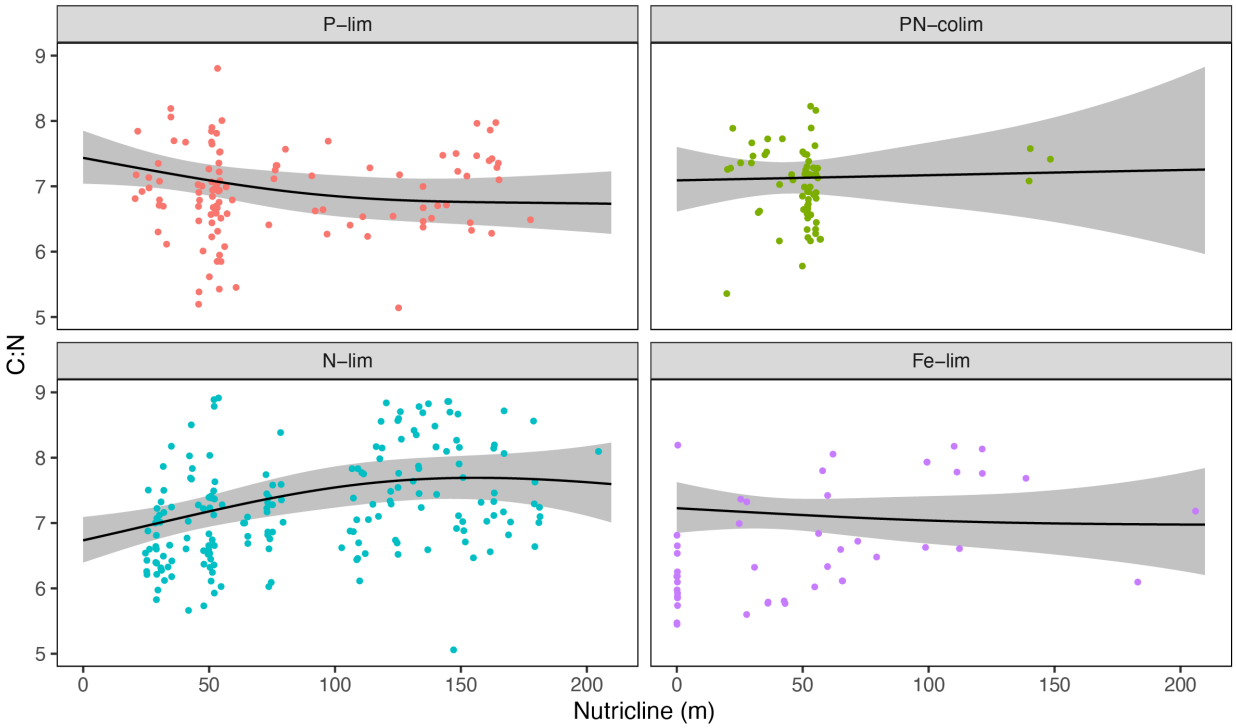

Extended Data Fig. 5: Observed C:N as a function of nutricline depth and nutrient limitation types. The figure is identical to main Fig. 3i but highlights the uncertainty (± 2SE) associated with GAM predictions under the constant SST and surface nitrate values.

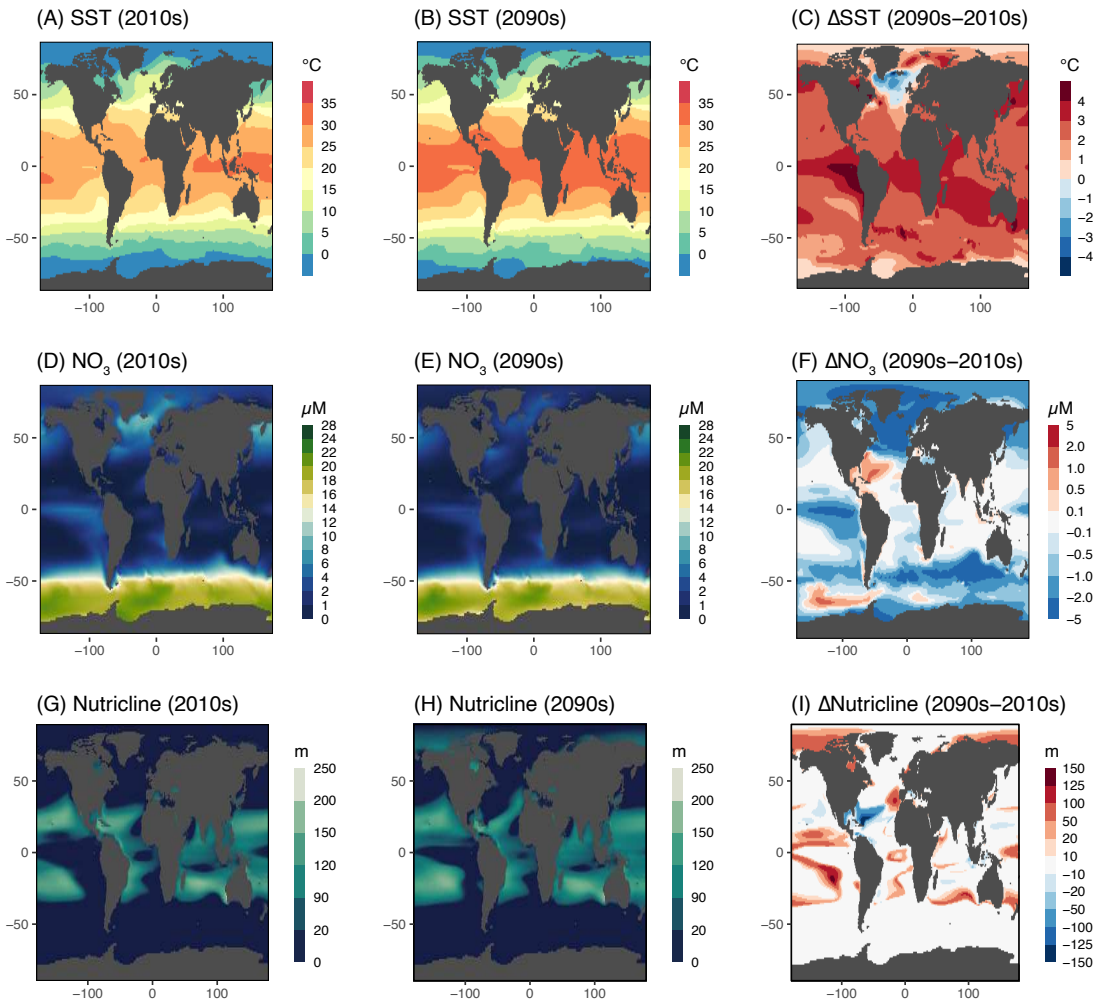

Extended Data Fig. 6: Modeled annual mean nutrient, temperature, and nutricline fields from CESM2-LENS for the historic periods (2010s) and the 2090s under the SSP3-7.0 scenario. The last column shows the difference between the 2090s and 2010s.

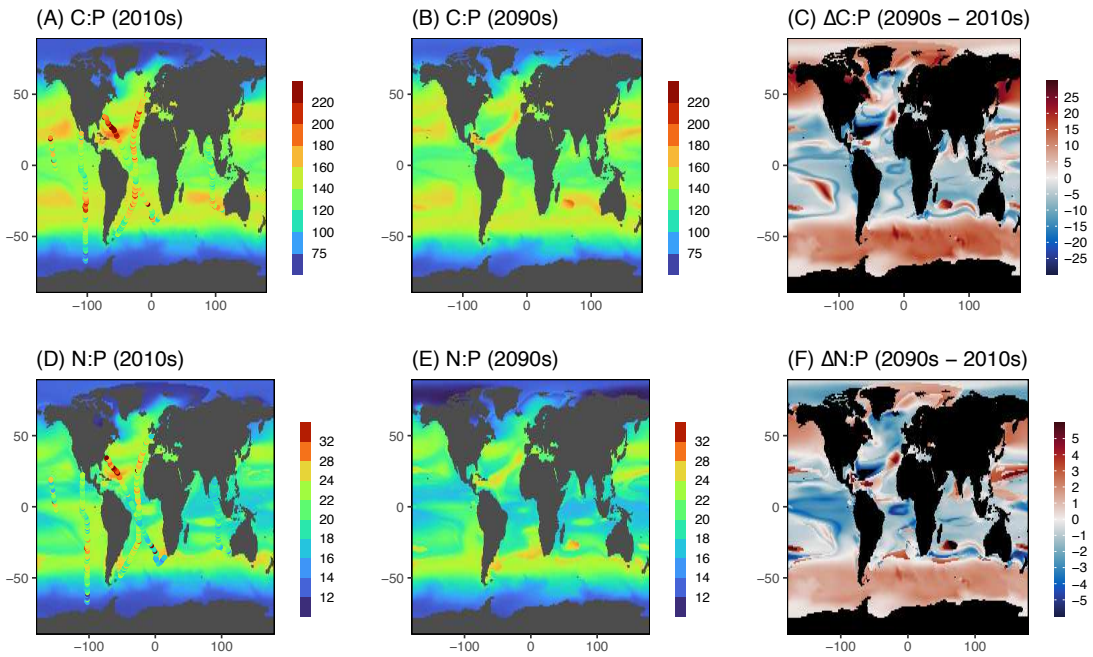

Extended Data Fig. 7: Modeled annual mean C:P and N:P for the historic periods (2010s) and the 2090s under the SSP3-7.0 scenario. C:P and N:P are computed by forcing data-derived GAMs with nutrient, temperature, nutricline, and nutrient limitation fields of small phytoplankton from CESM2-LENS. Colored dots in **(a)** and **(d)** are observed C:N:P from Bio-GO-SHIP cruises used in this study. The last column shows the difference between the 2090s and 2010s.

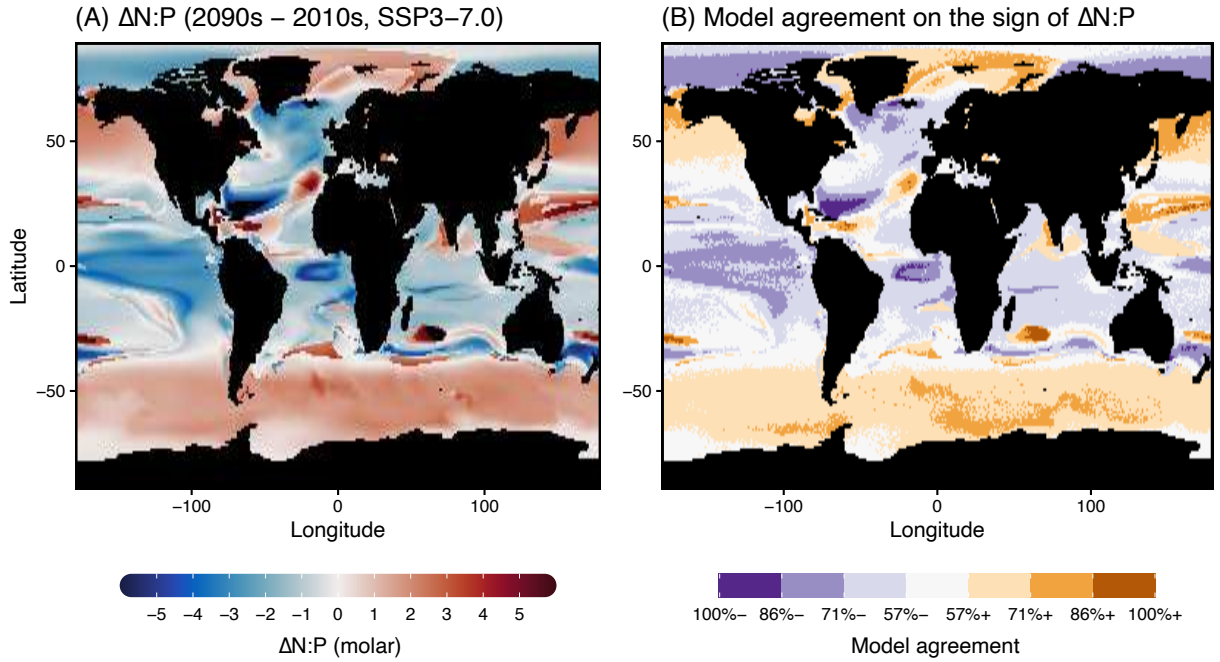

Extended Data Fig. 8: Projected impact of climate change on the surface community N:P. (**a**) The difference in surface community N:P estimated for the 2090s and 2010s based on SST, surface nitrate concentration, nutricline, and nutrient limitation of small phytoplankton simulated under the SSP3-7.0 and historic CMIP6 scenarios, respectively. (**b**) Model agreement on the sign of change in N:P amongst 2000 randomly generated model projections based on the posterior distribution of the GAM parameters. 100%+ represents the case when all 2000 models predict the positive change in N:P, and 100%- represents the case when all models predict the negative change in N:P. Note that 50%+/50%- corresponds to the minimum agreement between models.

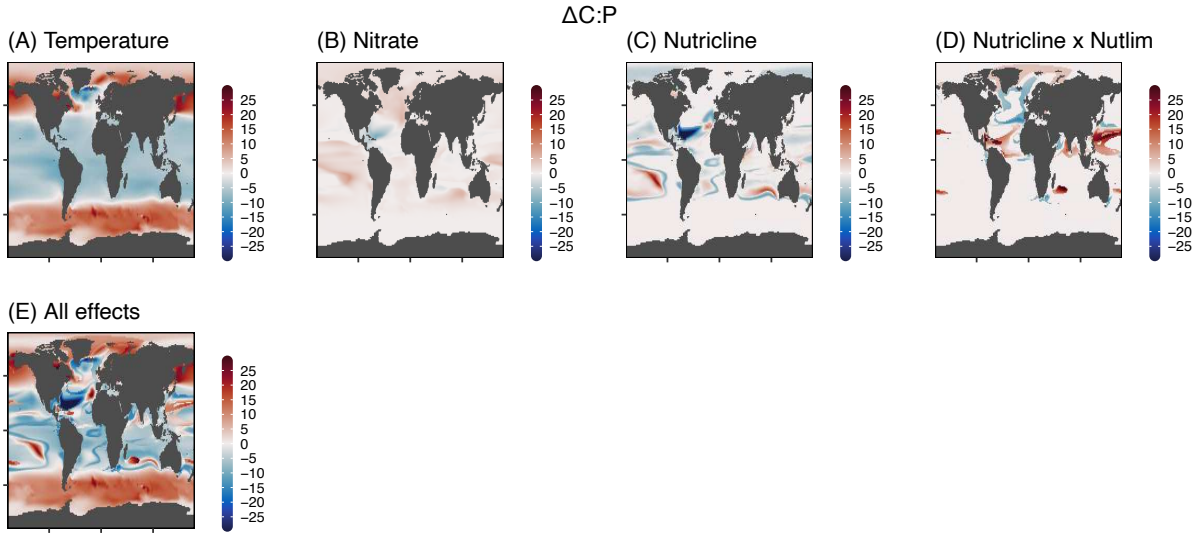

Extended Data Fig. 9: Evaluation of drivers of future C:P change. Impact of changes in (**a**) SST, (**b**) surface nitrate concentration, (**c**) nutricline depth, (**d**) nutrient limitation pattern, and (**e**) the combined effect (identical to Fig. 4a in the main text) for the change in community C:P from the 2010s to the 2090s under the SSP3-7.0 scenario.

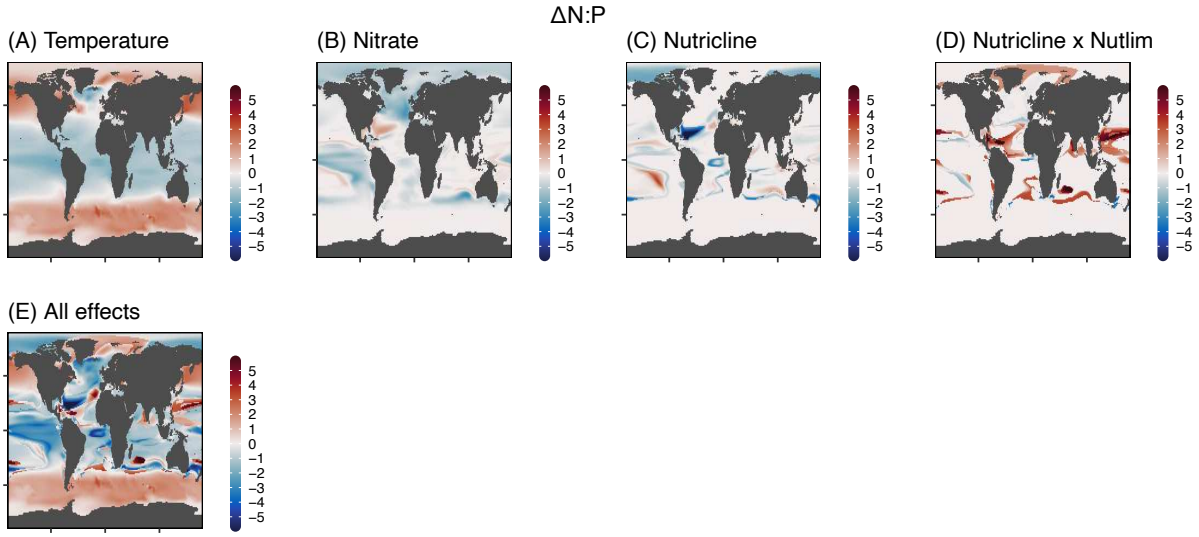

652
653 **Extended Data Fig. 10: Evaluation of drivers of future N:P change.** Impact of changes in (**a**) SST, (**b**) surface
654 nitrate concentration, (**c**) nutricline depth, (**d**) nutrient limitation pattern, and (**e**) the combined effect (identical to
655 Extended Data Fig. 8a) for the change in community N:P from the 2010s to the 2090s under the SSP3-7.0 scenario.
656

Supplementary Files

This is a list of supplementary files associated with this preprint. Click to download.

- Supportinginformation.pdf